Nanowire Orientation

DOI: 10.1002/anie.201408617

Large-Area Alignment of Tungsten Oxide Nanowires over Flat and Patterned Substrates for Room-Temperature Gas Sensing**

*Wei Cheng, Yanrui Ju, Payam Payamyar, Darinka Primc, Jingyi Rao, Christoph Willa, Dorota Koziej, and Markus Niederberger**

Abstract: *Alignment of nanowires over a large area of flat and patterned substrates is a prerequisite to use their collective properties in devices such as gas sensors. In this work, uniform single-crystalline ultrathin $W_{18}O_{49}$ nanowires with diameters less than 2 nm and aspect ratios larger than 100 have been synthesized, and, despite their flexibility, assembled into thin films with high orientational order over a macroscopic area by the Langmuir–Blodgett technique. Alignment of the tungsten oxide nanowires was also possible on top of sensor substrates equipped with electrodes. Such sensor devices were found to exhibit outstanding sensitivity to H_2 at room temperature.*

Metal oxide nanowires have been intensively studied in gas-sensing applications during the past decade because of their high surface to volume ratio, well-defined, one-dimensional geometry, and high crystallinity.[1–3] The sensors are based either on single nanowires[4] or on nanowire thin films.[5] Single nanowire sensors offer advantages such as superior sensing performance, miniaturization of the sensor device and low power consumption. But they are difficult to fabricate and suffer from problems such as low reproducibility and low mechanical stability. Compared to single nanowire sensors, nanowire thin films offer a higher potential for practical applications, because they can easily and reproducibly be prepared by wet chemical processes, such as drop casting, spin coating, or doctor blading. However, with these preparation approaches, the nanowires on the substrate are always randomly oriented with respect to each other, and hence, the geometrical advantage of the one dimensional morphology is not fully utilized. Therefore, it would be very attractive to fabricate thin-film sensors composed of oriented metal oxide nanowires aligned over the whole sensor substrate.

The Langmuir–Blodgett (LB) technique is particularly promising for the assembly of nanowires over a large area.[6] For example, it was shown that ultrathin Au nanowires could be assembled at the water–air interface over large areas allowing the study of bulk conductivity.[7] Liu et al. reported the LB assembly of flexible, ultralong Te nanowires for photoelectrical applications.[8] In those studies, the substrates for transferring the LB nanowire thin films were flat. However, in our case, the sensor substrates are not completely flat, because they have electrodes deposited on the surface, which are required for measuring the sensing properties. Such patterned surfaces represent an additional challenge for transferring the aligned nanowire thin film from the air–water interface to the sensor substrate without deterioration of the long-range order.

Being n-type semiconductors, tungsten oxides (WO_{3-x}) have promising applications as gas sensors, in electrochromic devices, or as photocatalysts.[9] Ultrathin (diameter less than 10 nm) tungsten oxide nanorods and nanowires have already been synthesized[10] and assembled for electrochromic applications.[11] However, to date, no successful attempts to align them for gas-sensing applications have been reported.

Herein, we report the synthesis of colloidally stable, ultrathin $W_{18}O_{49}$ nanowires, their alignment with high directional order over a macroscopic area and their H_2-sensing properties at room temperature. The nanowires are prepared by a facile solution method. They are single crystalline, with diameters of about 1.7 nm and aspect ratios larger than 100. Most importantly, they are highly dispersible in chloroform and chlorobenzene, enabling the use of these dispersions for alignment experiments by the LB technique. The flexible ultrathin nanowires can be successfully oriented over a large scale and transferred to Si/SiO_2 substrates patterned with Pt interdigitated electrodes. The aligned $W_{18}O_{49}$ nanowire thin films exhibit excellent sensing performance towards hydrogen in humid air, at room temperature, indicating their high potential for gas sensors.

The tungsten oxide nanowires were synthesized by heating a mixture of WCl_6, benzyl alcohol, and oleylamine at 180 °C for 24 h (see Supporting Information). The phase purity of the sample was analyzed by X-ray diffraction (XRD). As shown in Figure 1 a, it is difficult to unambiguously assign the pattern to a specific crystal phase among the many stoichiometric and nonstoichiometric tungsten oxides. Their structures and thus their patterns are quite similar and

[*] W. Cheng, Y. R. Ju, Dr. D. Primc, C. Willa, Dr. D. Koziej, Prof. Dr. M. Niederberger
Laboratory for Multifunctional Materials
Department of Materials, ETH Zurich
Vladimir-Prelog-Weg 5, 8093 Zurich (Switzerland)
E-mail: markus.niederberger@mat.ethz.ch
P. Payamyar, Dr. J. Y. Rao
Laboratory of Polymer Chemistry, Department of Materials
ETH Zurich, Vladimir-Prelog-Weg 5, 8093 Zurich (Switzerland)

[**] We thank ETH Zurich (ETH-28 13-1), the Swiss National Science Foundation (200021_140581), and the China Scholarship Council for financial support. We also thank Prof. A. Dieter Schlüter for providing access to the Langmuir–Blodgett trough. We acknowledge the use of equipment in the Scientific Center for Optical and Electron Microscopy (ScopeM) of the ETHZ and the Center for Electron Microscopy and Microanalysis (CEMM) of the Jožef Stefan Institute. We acknowledge Prof. U. Weimar and Dr. N. Barsan (University of Tuebingen (Germany)) for making their expertise in building gas-mixing stations available to us and Dr. A. Oprea (University of Tuebingen (Germany)) for setting-up the system.

Supporting information for this article is available on the WWW under http://dx.doi.org/10.1002/anie.201408617.

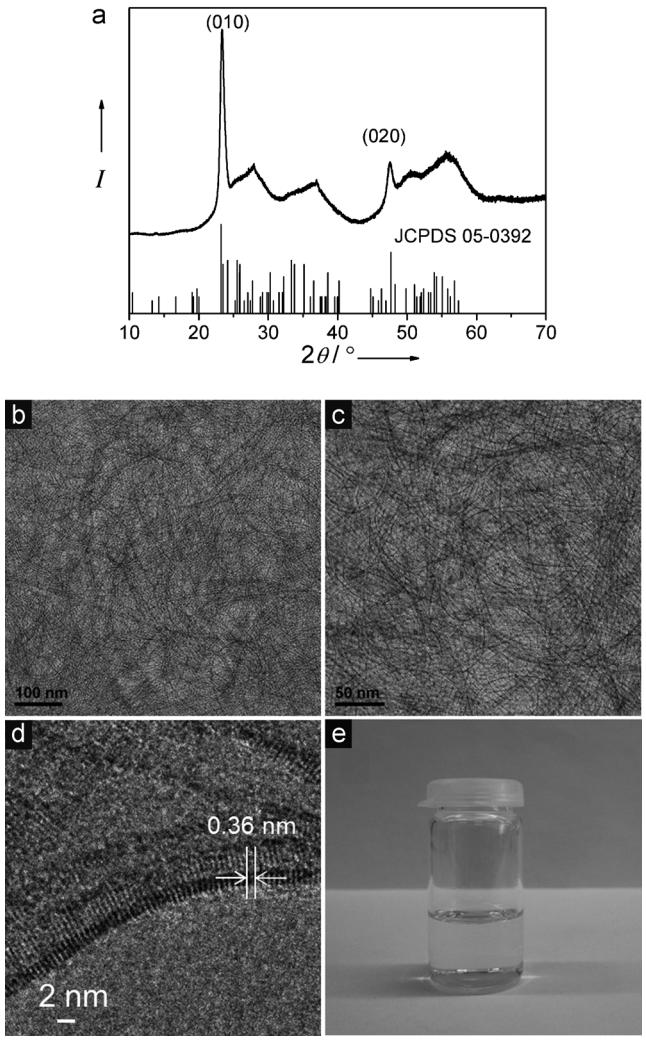

Figure 1. a) Representative XRD pattern of a tungsten oxide nanowire powder; b)–d) TEM images of the tungsten oxides nanowires: b) low magnification; c) high magnification; d) HRTEM image; e) Photograph of the tungsten oxide nanowires dispersed in chloroform (2 mg mL^{-1}).

our experimental diffractogram mainly consist of broad humps. Nevertheless, the pattern resembles those reported for $W_{18}O_{49}$ nanorods and nanowires bundles,[10a–d] matching best with monoclinic $W_{18}O_{49}$ (JCPDS 05-0392). There are two intensive peaks at $2\theta = 23.4°$ and 47.5°, which can be indexed to the (010) and (020) planes of the monoclinic $W_{18}O_{49}$, indicating that the nanowires grow along [010].

The freshly synthesized $W_{18}O_{49}$ nanowires suffered from severe aggregation. They were not dispersible in chloroform or other nonpolar solvents in spite of the oleylamine present in the reaction solution (Supporting Information, Figure S1). To separate the agglomerates into well-dispersed nanowires, a mixture of chloroform and oleylamine was added to the as-synthesized sample (no matter whether the product was wet or dry). The dispersion was sonicated for about 2 h until transparent. The nanowires were precipitated, washed, and finally redispersed in chloroform or chlorobenzene (for details see Supporting Information), forming transparent, colorless dispersions which were stable for months (Figure 1e). Figure 1b shows an overview TEM image of the dispersed nanowires at low magnification. The sample consists of a large number of highly uniform, ultrathin nanowires, which can be better seen in the image at higher magnification (Figure 1c). The nanowires are frequently bent and looped on the TEM grid, indicating their high flexibility. The HRTEM image (Figure 1d) shows that the nanowires are single crystalline with diameters of about 1.7 nm. The lattice spacing along the direction of the nanowires is about 0.36 nm, corresponding to the (010) lattice plane of $W_{18}O_{49}$, which suggests that the preferential growth direction of the nanowire is [010], consistent with the XRD analysis. The length of the nanowires reaches up to several hundred nanometers which means that the aspect ratio is more than 100.

Addition of oleylamine to the initial reaction mixture had a tremendous effect on the composition and on the morphology of the product. Without oleylamine, the reaction between WCl_6 and benzyl alcohol yielded a yellow powder consisting of WO_3 nanoplatelets (Figure S2). When oleylamine was added, the color of the product changed to dark blue, indicating a reduced tungsten oxide ($W_{18}O_{49}$) and the morphology changed from platelets to nanowires (Figure S3a). With an increasing amount of oleylamine, nanowires with higher aspect ratio were obtained (Figure S3b,c). Infrared spectroscopy confirmed the presence of oleylamine on the surface of the $W_{18}O_{49}$ nanowires (Figure S4). Using other long-chain alkyl amines, such as dodecylamine or octylamine, also resulted in ultrathin nanowires without any obvious changes in diameters and lengths (Figure S5a–d). Based on these observations we assume that the long-chain aliphatic amines serve as reducing and as capping agent, guiding the growth of the tungsten oxide in [010] direction.

Langmuir–Blodgett assembly of inorganic nanoparticles requires that the nanoparticles have hydrophobic surfaces so that they can float at the water–air interface.[6a] The oleylamine-capped $W_{18}O_{49}$ nanowires are hydrophobic and well dispersed in nonpolar solvents, which renders them suitable for the LB assembly. It turns out that the LB technique is an efficient way to organize the $W_{18}O_{49}$ nanowires into ordered patterns in spite of their structural flexibility. However, it is critically important to carefully elaborate the optimum experimental conditions to achieve a compact monolayer (for details, see Supporting Information). Figure S6a shows the surface pressure versus area isotherms of the nanowires floating on the water surface during the compression of the two barriers. At the initial stage, the decrease of the area barely influences the surface pressure. In stage II, the surface pressure rises slowly during the reduction of the surface area, indicating the formation of a LB monolayer. But the TEM image of this LB film reveals only loosely packed nanowires without specific orientation (Figure S6b). With further decrease of the surface area, the surface pressure rises steeply from 4 mN m^{-1} to about 26 mN m^{-1}. In this stage III, the loosely arranged nanowire arrays become more densely packed (Figure S6c), and the compression force generated by the barriers orients the nanowires parallel to the barrier. Finally, a compact, well-aligned nanowire monolayer film formed (Figure S6d). If the surface area is further decreased, the surface pressure continues to increase, but with a notice-

ably smaller gradient. In this case, overlaps and folds start to form and the thin film was no longer a monolayer (Figure S6e). These results indicate that the optimum condition to produce a well-aligned nanowire monolayer can be found in stage III at about 25 $mN\,m^{-1}$.

So far, we have demonstrated that our $W_{18}O_{49}$ nanowires can be aligned on the water–air interface. But to apply the aligned nanowire thin film in a device, it is necessary to find a suitable way to transfer it to a solid substrate. A flat silicon substrate (silicon wafer with thermally grown 400 nm SiO_2) was vertically dipped into the water (see Supporting Information). After the surface pressure reached 25 $mN\,m^{-1}$, the substrate was pulled up with a constant speed and the aligned nanowire thin film on the water surface was taken up by the substrate. As shown in Figure 2a, the front side of the substrate is perpendicular to the barriers. After compression, the nanowires on the water surface are oriented parallel to the barriers, thus, after transferring, the nanowires are expected to lie on the substrate as illustrated in Figure 2e. The SEM images show that the nanowire monolayer thin film homogeneously covers the substrate (Figure 2b).

Owing to the oleylamine coating, it is impossible to reveal any details of the nanowires by SEM. But AFM images at different magnifications clearly reveal that they are well-aligned over a large area, although some defects are still visible (Figure 2c,d). Most importantly, the nanowire thin films are very uniform and dense. Turning the substrate by 90°, so that the front side of the substrate is parallel to the barriers (Figure S7a), also yields homogeneous and well aligned nanowire films (Figure S7b–d), but with a different orientation (Figure S7e). These experiments show that the aligned tungsten oxide nanowire thin films can be transferred to solid substrates and their orientation on the substrate can easily be controlled.

The oleylamine capping on the surface of the nanowires is critical for the successful LB assembly, but at the same time it might have a detrimental effect on the application of these nanowires in electronic devices. Therefore, we developed a heat-treatment procedure that removed the oleylamine from the surface of the nanowires, but preserved the morphology of the assembled structures. Study of the dependence of the crystal structure of the nanowires on the annealing temperature (Figure S8) showed that 400 °C is the threshold temperature for the transformation of $W_{18}O_{49}$ to WO_3. Thus, 350 °C was selected as the calcination temperature, and indeed the compact, uniform, and well-aligned nanowire thin films are fully preserved after such heat treatment (Figure S9). According to IR spectroscopy data, the oleylamine was successfully removed from the surface of the nanowires (Figure S10).

To test the compatibility of our method with the use of the aligned nanowire films in electronic devices, we investigated the influence of patterned substrates on the morphology of the assemblies. The nanowires were assembled at the water–air interface by LB technique as described above, but then transferred to a silicon substrate equipped with 30 nm thick Pt interdigitated electrodes and annealed in air (see Supporting Information). The area with the Pt electrodes, extending over 7 × 4 mm, can be completely covered by a monolayer of aligned nanowires as shown in Figure S11. By repeating the LB deposition process, high quality multilayer thin films were produced as shown in Figure S12 and Figure 3. The local height differences on the substrate clearly do not affect the quality of the aligned nanowire thin film. The morphology of the layers on the patterned substrates is similar to that on the flat substrates. We anticipate that this is due to the aforementioned high bendability of the ultrathin nanowires and the high structural

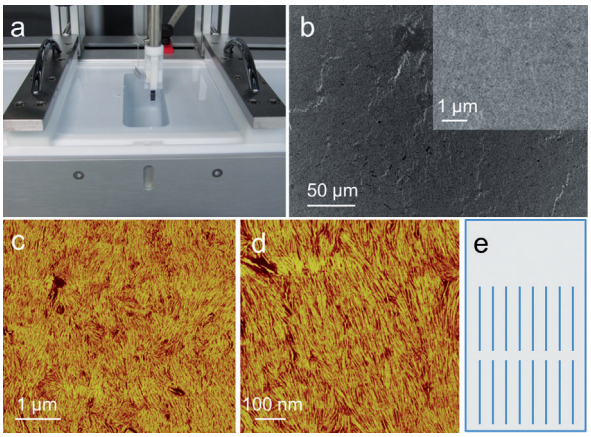

Figure 2. a) Photograph of the Langmuir–Blodgett trough with the silicon substrate oriented vertical to the barriers; b) SEM image of the transferred $W_{18}O_{49}$ nanowire thin film on the substrate; c,d) AFM images at different magnifications of the tungsten oxide nanowire thin film (phase image); e) illustration of the ideal arrangement of the nanowires on the substrate.

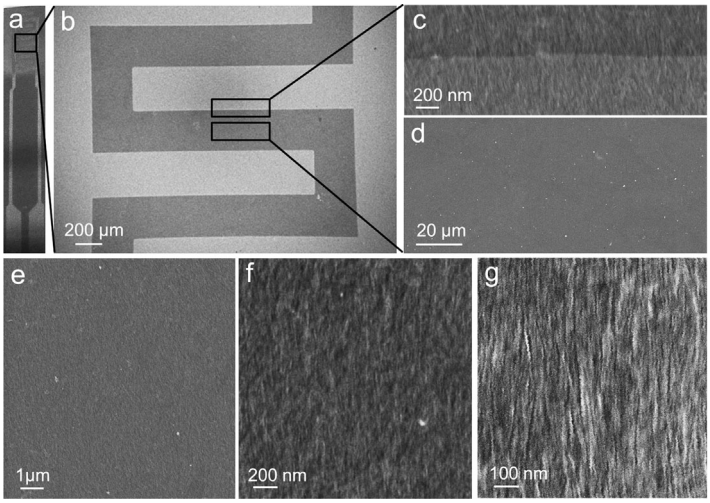

Figure 3. a) Digital photograph of the device coated with a film of 10 layers of aligned $W_{18}O_{49}$ nanowires on top of the interdigitated Pt electrodes; b) SEM image of the region highlighted with a rectangle in (a). The bright areas are the Pt interdigitated electrodes, dark areas the aligned nanowire thin film; c) SEM image of a region at the edge of one Pt electrode; d) SEM image of the nanowire thin film between the electrodes; e,f,g) SEM images of the nanowire thin film at higher magnifications (because the oleylamine was removed by calcination, it is possible to resolve the nanowires by SEM).

flexibility of the nanowire assemblies. They are stabilized by van der Waals interactions between the long alkyl chains of the oleylamine molecules adsorbed at the surface, which become increasingly interdigitated, and thus more attractive, with increasing compression.

Based on all these findings, our fabrication procedure seems to be suitable for the incorporation of the aligned nanowire layers into electronic devices. As a proof-of-concept, we utilized the assembled nanowire thin films in chemoresistive gas sensors. Tungsten oxide is known to respond to reducing gases, such as H_2, H_2S, or to oxidation gases, such as NO_x, at elevated temperatures ranging from 150 to 400 °C.[12] Examples reporting the application of tungsten oxide as a H_2 sensor operating at temperatures below 60 °C are rare and limited to sensing of relatively high concentrations of over 500 ppm.[13] Because the performance of nanowire-based devices, fabricated by the LB technique, is often dependent on the number of layers,[8,11b,14] we measured the resistance changes of sensor films composed of one, three, and ten layers of aligned $W_{18}O_{49}$ nanowires upon exposure to different concentrations of H_2 at room temperature. We found that a three-layers-thick film was the minimum to detect H_2 (Figure S13). However, the highest sensor signal and the best baseline stability were measured with the sensors composed of ten layers as shown in Figure 4a. Additionally, the positive cross-sensitivity to humidity below 75% relative humidity (RH) is observed (Figure S14). At 50% RH, the 10-layers sensor exhibits the optimum performance in terms of sensing signal, response, and recovery time, with a linear response and sensitivity of 0.145 ppm^{-1} (Figure 4b) in the range 2–100 ppm H_2. The sensor also exhibits good repeatability as shown in Figure 4c. This high sensor performance reflects the unique properties of our aligned $W_{18}O_{49}$ nanowire layers. We assume that the performance of the assemblies of ultrathin $W_{18}O_{49}$ nanowires as a sensitive layer results from: a) a high conductivity along the aligned nanowires necessary for efficient operation of the sensors, b) a high surface area necessary for the reliable detection of low H_2 concentrations, and c) a high concentration of oxygen vacancies that provide adsorption sites for H_2 in the lattice of the ultrathin non-stoichiometric tungsten oxide nanowires.

In conclusion, we successfully synthesized single-crystalline ultrathin $W_{18}O_{49}$ nanowires with high aspect ratio by an aliphatic amine assisted benzyl alcohol route. The nanowires can be processed into stable, colorless, and transparent dispersions in nonpolar solvents, such as chloroform or chlorobenzene. The high colloidal stability of the nanowires makes it possible to assemble them by the Langmuir–Blodgett technique into homogeneous, compact films oriented over a large area and with varying thickness. Despite the patterned surface of the sensor substrate, the aligned nanowire thin films can be successfully transferred onto it. The sensor, composed of 10 layers of aligned nanowires, shows excellent room-temperature sensitivity to H_2 in humid air. The strategy developed herein is one of the few examples in which nanoscale building blocks are successfully integrated into a macroscopic device.[6d,8,11b] It shows how important the arrangement of metal oxide nanoparticles over all length scales is.[15]

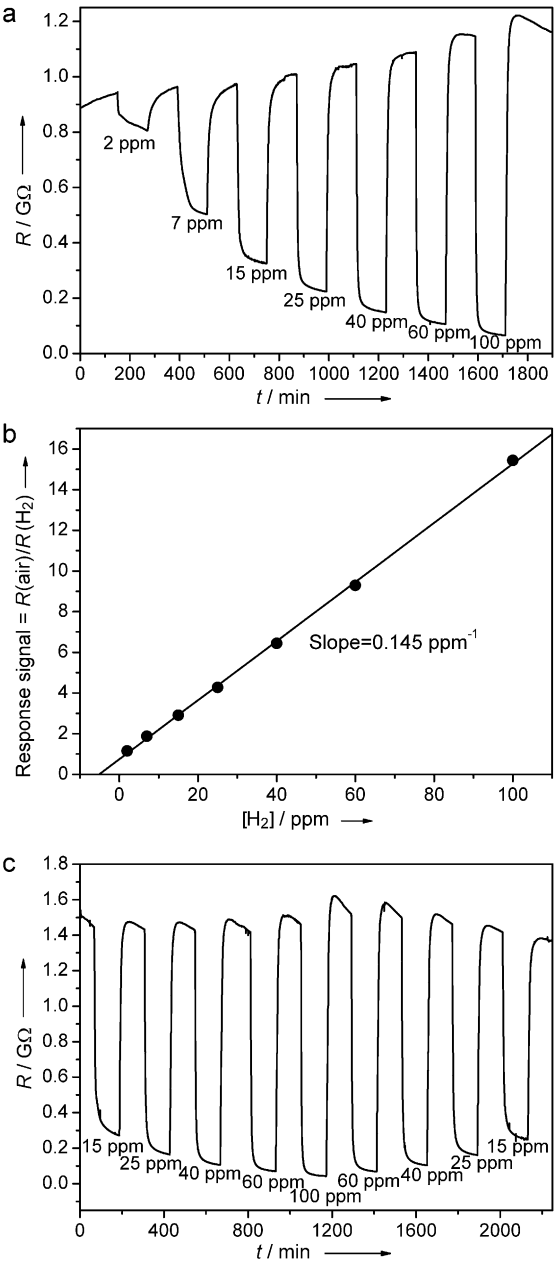

Figure 4. a) Resistance change, b) response signal, and c) repeatable sensing measurement of aligned $W_{18}O_{49}$ nanowire thin films (10 layers) with respect to various concentrations of H_2 at room temperature in synthetic air with 50% relative humidity as carrier gas.

Received: August 27, 2014
Published online: November 20, 2014

Keywords: hydrogen sensing · Langmuir–Blodgett technique · nanowires · sensors · tungsten

[1] E. Comini, C. Baratto, G. Faglia, M. Ferroni, A. Vomiero, G. Sberveglieri, *Prog. Mater. Sci.* **2009**, *54*, 1–67.
[2] E. Comini, G. Sberveglieri, *Mater. Today* **2010**, *13*, 36–44.
[3] X. Chen, C. K. Y. Wong, C. A. Yuan, G. Zhang, *Sens. Actuators B* **2013**, *177*, 178–195.

[4] a) M. Law, H. Kind, B. Messer, F. Kim, P. Yang, *Angew. Chem. Int. Ed.* **2002**, *41*, 2405 – 2408; *Angew. Chem.* **2002**, *114*, 2511 – 2514; b) A. Kolmakov, Y. Zhang, G. Cheng, M. Moskovits, *Adv. Mater.* **2003**, *15*, 997 – 1000; c) D. Zhang, Z. Liu, C. Li, T. Tang, X. Liu, S. Han, B. Lei, C. Zhou, *Nano Lett.* **2004**, *4*, 1919 – 1924; d) S. H. Jeong, S. Kim, J. Cha, M. S. Son, S. H. Park, H. Y. Kim, M. H. Cho, M. H. Whangbo, K. H. Yoo, S. J. Kim, *Nano Lett.* **2013**, *13*, 5938 – 5943.

[5] a) Q. Wan, Q. H. Li, Y. J. Chen, T. H. Wang, X. L. He, J. P. Li, C. L. Lin, *Appl. Phys. Lett.* **2004**, *84*, 3654 – 3656; b) Y. S. Kim, S. C. Ha, K. Kim, H. Yang, S. Y. Choi, Y. T. Kim, J. T. Park, C. H. Lee, J. Choi, J. Paek, K. Lee, *Appl. Phys. Lett.* **2005**, *86*, 213105; c) Y. M. Zhao, Y. Q. Zhu, *Sens. Actuators B* **2009**, *137*, 27 – 31; d) I. S. Hwang, E. B. Lee, S. J. Kim, J. K. Choi, J. H. Cha, H. J. Lee, B. K. Ju, J. H. Lee, *Sens. Actuators B* **2011**, *154*, 295 – 300.

[6] a) A. R. Tao, J. X. Huang, P. D. Yang, *Acc. Chem. Res.* **2008**, *41*, 1662 – 1673; b) S. Acharya, J. P. Hill, K. Ariga, *Adv. Mater.* **2009**, *21*, 2959 – 2981; c) M. C. P. Wang, B. D. Gates, *Mater. Today* **2009**, *12*, 34 – 43; d) J. W. Liu, H. W. Liang, S. H. Yu, *Chem. Rev.* **2012**, *112*, 4770 – 4799.

[7] Y. Chen, Z. Ouyang, M. Gu, W. Cheng, *Adv. Mater.* **2013**, *25*, 80 – 85.

[8] J. W. Liu, J. H. Zhu, C. L. Zhang, H. W. Liang, S. H. Yu, *J. Am. Chem. Soc.* **2010**, *132*, 8945 – 8952.

[9] H. Zheng, J. Z. Ou, M. S. Strano, R. B. Kaner, A. Mitchell, K. Kalantar-zadeh, *Adv. Funct. Mater.* **2011**, *21*, 2175 – 2196.

[10] a) K. Lee, W. S. Seo, J. T. Park, *J. Am. Chem. Soc.* **2003**, *125*, 3408 – 3409; b) J. Polleux, A. Gurlo, N. Barsan, U. Weimar, M. Antonietti, M. Niederberger, *Angew. Chem. Int. Ed.* **2006**, *45*, 261 – 265; *Angew. Chem.* **2006**, *118*, 267 – 271; c) A. Yella, M. N. Tahir, S. Meuer, R. Zentel, R. Berger, M. Panthofer, W. Tremel, *J. Am. Chem. Soc.* **2009**, *131*, 17566 – 17575; d) G. Xi, S. Ouyang, P. Li, J. Ye, Q. Ma, N. Su, H. Bai, C. Wang, *Angew. Chem. Int. Ed.* **2012**, *51*, 2395 – 2399; *Angew. Chem.* **2012**, *124*, 2445 – 2449; e) B. Moshofsky, T. Mokari, *Chem. Mater.* **2013**, *25*, 1384 – 1391.

[11] a) S. J. Yoo, J. W. Lim, Y. E. Sung, Y. H. Jung, H. G. Choi, D. K. Kim, *Appl. Phys. Lett.* **2007**, *90*, 173126; b) J. W. Liu, J. Zheng, J. L. Wang, J. Xu, H. H. Li, S. H. Yu, *Nano Lett.* **2013**, *13*, 3589 – 3593.

[12] a) P. J. Shaver, *Appl. Phys. Lett.* **1967**, *11*, 255 – 257; b) S. J. Ippolito, S. Kandasamy, K. Kalantar-zadeh, W. Wlodarski, *Sens. Actuators B* **2005**, *108*, 154 – 158; c) M. Ahsan, M. Z. Ahmad, T. Tesfamichael, J. Bell, W. Wlodarski, N. Motta, *Sens. Actuators B* **2012**, *173*, 789 – 796; d) A. Ponzoni, E. Comini, G. Sberveglieri, J. Zhou, S. Z. Deng, N. S. Xu, Y. Ding, Z. L. Wang, *Appl. Phys. Lett.* **2006**, *88*, 203101 – 203103; e) D. Meng, N. M. Shaalan, T. Yamazaki, T. Kikuta, *Sens. Actuators B* **2012**, *169*, 113 – 120.

[13] a) R. Calavia, A. Mozalev, R. Vazquez, I. Gracia, C. Cané, R. Ionescu, E. Llobet, *Sens. Actuators B* **2010**, *149*, 352 – 361; b) Y. Shen, T. Yamazaki, Z. Liu, D. Meng, T. Kikuta, N. Nakatani, *Thin Solid Films* **2009**, *517*, 2069 – 2072.

[14] J. W. Liu, J. Xu, H. W. Liang, K. Wang, S. H. Yu, *Angew. Chem. Int. Ed.* **2012**, *51*, 7420 – 7425; *Angew. Chem.* **2012**, *124*, 7538 – 7543.

[15] D. Koziej, A. Lauria, M. Niederberger, *Adv. Mater.* **2014**, *26*, 235 – 257.

